

Nonthermal transient phenomena around rotating black holes

Maurice H.P.M. van Putten

Abstract Ultra-high energy cosmic rays (UHECRs) and gamma-ray bursts (GRBs) are the most exceptional events known in the Transient Universe. They are non-thermal, and appear to be associated with black holes. Here, we describe radiation mechanisms induced by flows in forced turbulence around rapidly rotating black holes: high-energy emissions from a relativistic capillary effect along the black hole spin-axis and low-energy emissions by catalytic conversion of spin-energy. The latter is dominant, whereby it sets the evolution and lifetime of black hole spin and, hence, the light curves of the high-energy emissions. High-energy emissions arise, concurrently, in photons from dissipation in a baryon-poor jet extracted by the capillary effect and, upstream of an outgoing Alfvén front, in ionic contaminants by linear acceleration. These contaminants develop into ultra-high energy cosmic rays (UHECRs) about the Greisen-Zatsepin-Kuzmin (GZK) threshold in low-luminosity, intermittent active galactic nuclei. These may include Seyfert galaxies and Cen A as suggested by recent detections of UHECRs by the Pierre Auger Observatory and, for the latter, also of Very High Energy (VHE) gamma-rays by the High Energy Stereoscopic System (HESS). Nearly complete spin-down of stellar mass black holes represents a common process in collapsars and mergers of neutron stars with another neutron star or companion black hole. Long GRBs from dissipative jets produced by rotating black holes hereby explain events with and without supernovae and a diversity in their X-ray afterglows. They have an intrinsic exponential decay in their light curves which is remarkably consistent with the average of 600 long GRBs by application of matched filtering, whose total output agrees with existing statistics on peak and true energies in gamma-rays. We conclude that long GRBs are spin-powered, not accretion-powered. Gravitational radiation from turbulent flows in SgrA* might be of interest to the planned Laser Interferometric Space Antenna (LISA) and, for stellar mass black holes in GRBs, should be detectable by LIGO-Virgo. Long GRBs from naked inner engines produced in mergers produce long-duration radio-burst that may be seen in all-sky surveys by the Low Frequency Array (LOFAR).

Le Studium IAS, 3D Avenue de la Recherche, 45071 Orléans Cedex 2, France, e-mail: mvp@ligo.mit.edu

1 Introduction

Recent high-energy observations reveal a Transient Universe abundant in nonthermal emissions, from ultra-high energy cosmic rays (UHECRs) from nearby sources recently detected by the Pierre Auger Observatory (PAO) [1, 2, 91], cosmological gamma-ray bursts and supernovae to, possibly, extragalactic radio-bursts [51].

The most exceptional non-thermal emissions appear to harbor black holes. Black holes have been widely recognized for providing natural sites for conversion of (baryon-free) gravitational energy into various emissions, by the release of binding energy and/or spin-energy in their angular momentum in, respectively, accretion and spin-powered nuclei.

Gravitation is not only shaping the large scale structure and cosmological evolution of the universe, but also governs some of the transient behavior on galactic scales down to that of stellar mass compact objects. The latter offers perhaps the best opportunity for probing in detail the non-Newtonian aspects of gravitation. It poses observational challenges which invite novel methods of data-analysis, probes in neutrino emissions, gravitational-waves and radio.

In this invited Lecture, I discuss rotating black holes as inner engines to burst and transient sources. Black holes are described merely by their mass and angular momentum, typically with a modest electric charge in their lowest energy state when rotating rapidly. As such, it becomes of interest to identify some of the relevant physical principles and scaling laws governing their evolution and radiation processes, and to compare their consequences with recent observations with an outlook to future observations.

My focus is on nonthermal emissions induced by flows in forced turbulence around rapidly rotating black holes [79]. This models gives rise to a variety of nonthermal emissions powered by the spin-energy of a black hole, directly and indirectly. In an astrophysical environment, black holes that are spun-down by surrounding matter introduce a new long-duration timescale that is intrinsic to an inner engine – the lifetime of rapid spin of the black hole. It sets the duration and light curves of high-energy emissions that may ensue along their spin-axis.

Our model has some power of unification, of ultra-high energy cosmic rays (UHECRs) from supermassive black holes and gamma-ray bursts (GRBs) from stellar mass black holes, and it some predictive power with regards to upcoming observations in gravitational radiation by the planned Laser Interferometric Space Antenna (LISA), the ground-based observatories LIGO-Virgo and, in the radio, the Low Frequency Array (LOFAR). This future outlook promises to directly probe matter and turbulence in the inner most regions around black holes.

In §2, we review some of the physical properties of Kerr black holes. In §3, we describe the causal physical processes driving radiation, in open outflows along the spin axis and, side-ways, onto surrounding matter. We apply these two processes to the problem of UHECRs in §4 and GRBs in §5, with some discussion on accretion-powered versus the present spin-powered model. The model has some power of unification, discussed in §6, and some predictive power for future observations by LISA, and LIGO-Virgo/LOFAR pointed out in §7.

2 Some physical properties of Kerr black holes

The Kerr metric [41] describes rotating black holes by their mass M , angular momentum J and specific angular momentum $a = J/M$. The various physical properties can be conveniently expressed in the trigonometric representation $\sin \lambda = a/M$ [79], shown in Table (1). In particular, the spin-energy [86] can be expressed untuitively as

$$E_{spin} = \frac{1}{2} \Omega_H^2 I f_s^2 \quad (1)$$

with

$$f_s = \frac{\cos(\lambda/2)}{\cos(\lambda/4)}, \quad \Omega_H = \frac{1}{2M} \tan(\lambda/2). \quad (2)$$

$I = 4M^3$ denotes the moment of inertia of slow rotation[75] and $0.7654 \leq f_s \leq 1$ is a moderation associated with arbitrary spin rates. Because (1) involves no small parameter, E_{spin}/M can be large, up to 29%. This is an order of magnitude larger than the spin energy of a neutron star.

SYMBOL	EXPRESSION	COMMENT
r_H	$2M \cos^2(\lambda/2)$	horizon radius
Ω_H	$\tan(\lambda/2)/2M$	angular velocity
E_{spin}	$2M \sin^2(\lambda/4)$	spin-energy, $< 0.29M$
M_{irr}	$M \cos(\lambda/2)$	irreducible mass, $> 0.71M$
A_H	$16\pi M_{irr}^2$	surface area
S_H	$4\pi M^2 \cos^2(\lambda/2)$	entropy
T_H	$\cos^2 / 8M \cos^2(\lambda/2)$	temperature
μ_H	QJ/M	Carter's magnetic moment[17]
Q_e	$\simeq 2BJ$	Wald's equilibrium charge[94]
$V_F(\theta)$	$e\Omega_H A_\phi(\theta)$	Fermi-level at poloidal angle θ [80]

Table 1 Parameters of the Kerr metric in Boyer-Lindquist coordinates, of mass M and angular momentum $J = M^2 \sin \lambda$ in geometrical units (Newton's constant and the velocity of light equal to 1) and $\hbar = 1$. Exposed to a vector potential A_a with magnetic field-strength B , we further encounter Q_e and an horizon Fermi-level V_F of particles of charge e .

A Kerr black hole in an astrophysical environment evolves according to the first law of thermodynamics

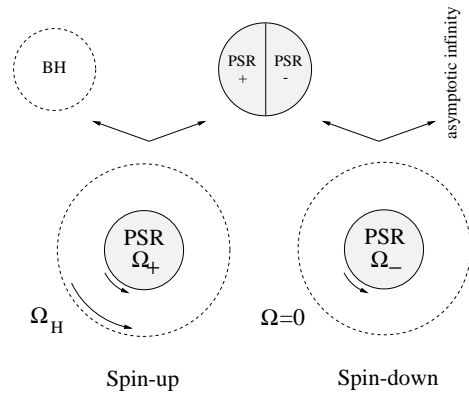
$$dM = \Omega_H dJ + T_H dS, \quad (3)$$

where T_H denotes the temperature of the event horizon, associated with a change $\Omega_H dJ$ in spin energy and a dissipation $dQ = T_H dS$ associated with the creation of Bekenstein-Hawking entropy [10] $S_H = 4\pi M^2 \cos^2(\lambda/2)$. Note that S_H can maximally *double* in the process of viscous spin-down of an initially rapidly spinning black hole.

3 Energetic processes by frame-dragging and Mach's principle

By Mach's principle, spacetime around rotating black holes is dragged along with the angular momentum of the black hole. This is apparent in frame-dragging: the angular velocity ω of particles with zero-angular momentum (relative to infinity; see [75] for a detailed discussion). Geometrically, the state of zero-angular momentum particles corresponds to world-lines that are orthogonal to slices of constant time-at-infinity, as described in the Boyer-Lindquist coordinates for the Kerr metric. Frame-dragging is differential, in that it decays with the cube of the distance to the black hole, whereby it is not a gauge effect. For radiative processes, Mach's principle attributes a symmetric role to the event horizon of a black hole and infinity, in view of their radiative ingoing and, respectively, outgoing boundary conditions. When the black hole is rotating, it introduces the following non-Newtonian interactions unique to the Kerr metric:

- a force (dimensionless in geometrical units) arising out of the product of angular momentum J [cm^2] and the Riemann tensor [cm^{-2}] [63, 86, 11]. Integration of this force produces a powerful capillary effect, extracting charged particles along open magnetic flux-tubes supported by the equilibrium magnetic moment of a black hole [86];
- an equivalence between spin-up of a disk by radiation onto a rapidly rotating black hole with spin-down of pulsars by radiation to infinity, schematically shown in Fig.(1). It implies catalytic conversion of black hole spin-energy into radiation to infinity in various emission channels, in spin-down against surrounding turbulent matter [79] accompanied by entropy creation in the event horizon.



a black hole and infinity, in view of their radiative ingoing and, respectively,

Fig. 1 Mach's principle attributes a symmetric role to the event horizon of outgoing boundary conditions. It implies an equivalence between radiation onto a rapidly rotating black hole by surrounding matter, and radiation to infinity by a pulsar. A torus, represented by its inner (PSR+) and outer (PSR-) faces, hereby produces catalytic conversion of spin-energy into various emission channels (Reprinted from [83].)

In what follows, we focus on rotating black holes surrounded a torus or disk that is uniformly magnetized, i.e., which carries a net poloidal magnetic flux that has nonzero variance in the presence of time-variability. This (instantaneous) magnetic flux can be represented by two counter-oriented current rings or, equivalently by Stokes' theorem, a uniform distribution of magnetic dipoles [83]. The torus hereby submerges the black hole in an approximately uniform magnetic field, whereby it assumes a net magnetic moment in its lowest energy state [94, 20]. It corresponds to the minimum $Q = BJ(r_H/M)$ of [81]

$$\mathcal{E} \simeq \frac{1}{2}CQ^2 - \mu_H B. \quad (4)$$

Here, $C \simeq 1/r_H$ denotes the electrostatic capacitance for of the black hole of size r_H , B the strength of the poloidal magnetic field and, by Carter's theorem [17], $\mu_H = QJ/M$ for a black hole with charge Q . The equilibrium magnetic moment serves to preserve essentially maximal magnetic flux through the event horizon at all spin-rates and it allows the black hole to support open magnetic field-lines, even in a state of suspended accretion [81]. This equilibrium state bears out well also in numerical simulations in the force-free approximation [42].

The energy \mathcal{E}_B in net poloidal magnetic flux supported by flows around black holes is subject to a stability bound [83]

$$\frac{\mathcal{E}_B}{\mathcal{E}_k} \leq \frac{1}{15} \quad (5)$$

relative to the kinetic energy \mathcal{E}_k of the torus. It bears out well also in a numerical toy model of a uniformly magnetized torus [15]. More generally, it may develop out of instabilities of hydrodynamic [64, 84] and magnetohydrodynamic origin [90, 18, 7].

Rotating flows in forced turbulence due to competing torques acting on the inner and the outer face of the torus [79] are in many ways similar though not identical to Taylor-Couette flows. With rigid boundaries, incompressible Taylor-Couette flows display an onset to turbulent flows by helical magnetic fields as expected [73].

3.1 A gravitational spin-orbit energy $E = \omega J$

From a position r in Boyer-Lindquist coordinates (t, r, θ, ϕ) along the spin-axis of a black hole, the line-integral of the above-mentioned force is [86, 87]

$$\mathcal{E}(r, \theta) = \int_r^\infty \text{Riemann} \times J_p ds = \omega(r, \theta) J_p, \quad (6)$$

where $\omega(r, \theta)$ refers to the frame-dragging angular velocity at (r, θ) , and J_p denotes the conserved angular momentum of the test particle. Applied to a charged particle, $J_p = eA_\phi$ along an open tube with magnetic flux $2\pi A_\phi$, \mathcal{E} can be arbitrarily large, depending on the magnetic field-strength and size of the black hole.

We can derive (6) as follows, in the approximation of small θ . Gravitational spin-spin interactions along a common spin-axis are such that anti-parallel spins attract, while parallel spins repel. Thus, an object whose spin is parallel to that of our planet weighs less than the same object with opposite spin. Based on dimensional analysis, we expect a gravitational potential for spin aligned interactions given by $E = \omega J_p$. To be precise, the non-zero components of the Riemann tensor of the Kerr metric can be expressed relative to a frame of tetrad 1-forms

$$e_{(0)} = \alpha dt, \quad e_{(1)} = \frac{\Sigma}{\rho}(d\phi - \omega dt) \sin \theta, \quad e_{(2)} = \frac{\rho}{\sqrt{\Delta}} dr, \quad e_{(3)} = \rho d\theta \quad (7)$$

as [16]

$$\begin{aligned} R_{0123} &= A \\ R_{1230} &= AC \\ R_{1302} &= AD \\ -R_{3002} &= R_{1213} = -A3a\sqrt{\Delta}\Sigma^{-2}(r^2 + a^2) \sin \theta \\ -R_{1220} &= R_{1330} = -B3a\sqrt{\Delta}\Sigma^{-2}(r^2 + a^2) \sin \theta \\ -R_{1010} &= R_{2323} = B = R_{0202} + R_{0303} \\ -R_{1313} &= R_{0202} = BD \\ -R_{1212} &= R_{0303} = -BC, \end{aligned} \quad (8)$$

where

$$\begin{aligned} A &= aM\rho^{-6}(3r^2 - a^2 \cos^2 \theta), \\ B &= Mr\rho^{-6}(r^2 - 3a^2 \cos^2 \theta), \\ C &= \Sigma^{-2}[(r^2 + a^2)^2 + 2a^2\Delta \sin^2 \theta], \\ D &= \Sigma^{-2}[2(r^2 + a^2)2 + a^2\Delta \sin^2 \theta]. \end{aligned} \quad (9)$$

Notice that on-axis $\theta = 0$,

$$2A = -\partial_r \omega = \frac{2aM}{\rho^6}(3r^2 - a^2), \quad C = 1, D = 2. \quad (10)$$

This brings about explicitly black hole-spin induced curvature components in the first three of (8) along the axis of rotation, and hence an implied curvature-spin connection. This interaction bears out by inspection of [63, 65]

$$F_2 = \frac{1}{2} \varepsilon_{abef} R_{cd}^{cf} J^a u^b u^d \quad (11)$$

evaluated in an orthonormal tetrad,

$$F_2 = JR_{3120} = JAD = -\partial_2 \omega J. \quad (12)$$

Line-integration gives the desired result

$$\mathcal{E} = \int_r^\infty F_2 ds = \omega J. \quad (13)$$

The result (13) may also be recognized, by considering the difference in total energy between particles which orbit the axis of rotation of the black hole with opposite spin. Let u^b denote the velocity four-vector and $\Omega = u^\phi/u^t$ denote the angular velocities of either one of these. Then the normalization

$$-1 = u^c u_c = [g_{tt} + g_{\phi\phi}\Omega(\Omega - 2\omega)] (u^t)^2 \quad (14)$$

has the two roots

$$\Omega_{\pm} = \omega \pm \sqrt{\omega^2 - (g_{tt} + (u^t)^{-2})/g_{\phi\phi}}. \quad (15)$$

For two particles with the same angular momentum except for a sign,

$$J_{\pm} = g_{\phi\phi}u^t(\Omega_{\pm} + \omega) = g_{\phi\phi}u^t \sqrt{\omega^2 - (g_{tt} + (u^t)^{-2})/g_{\phi\phi}} = \pm J \quad (16)$$

shows that u^t is the same for each particle. The total energy of the particles satisfies $E_{\pm} = (u^t)^{-1} + \Omega_{\pm}J_{\pm}$, whereby one-half the difference satisfies

$$\mathcal{E} = \frac{1}{2}(E_+ - E_-) = \omega J. \quad (17)$$

The curvature-spin coupling (13) is gravitational, and hence universal, i.e., it applies to angular momentum of mechanical or electromagnetic origin, as in $J_p = eA_\phi$.

The maximal horizon potential $E(r_H)$ in (6) equals the horizon Fermi-level: the chemical potential of charged in Hawking radiation in the presence of an electromagnetic vector potential [80, 86].

The environment of astrophysical black holes is expected to be abundant in e^\pm by canonical pair-cascade processes [13], so that these do not have to be created by vacuum break-down, see further [45]. Thus, (6) gives rise to a capillary effect [86]: the extraction of a leptonic outflow from the e^\pm -magnetosphere around the black hole into an outflow to infinity. It is expected to be launched in a nearly force-free and dissipationless state [13]. As an open outflow, it terminates in an outgoing Alfvén front, which then mediates the maximal potential energy $E(r_H, \theta)$ out to large distances (apart from moderation factors, due to the finite horizon impedance of the event horizon [75]). Magnetic flux-surfaces *upstream* of the Alfvén front remain largely charge-free, and become a linear accelerator.

The capillary effect is closely related to the induction of a nonzero invariant $E \cdot B$ associated with an EMF of the vacuum electromagnetic field by frame-dragging [94, 86]. While charge equilibration to a force-free state [13] produces a leptonic outflow up to an outgoing Alfvén front, it does not effect the total EMF over semi-infinite loops connecting the event horizon and infinity, i.e., from the outgoing Alfvén front to infinity, since it effectively mediates the horizon Fermi-level in the force-free, dissipationless limit.

3.2 Evolution of black hole spin interacting with matter

Frame-dragging induces a powerful interaction between the black hole and a surrounding, uniformly magnetized torus. This can be seen by inspection of Faraday's equation in the Boyer-Lindquist coordinates of the Kerr metric. Let F_{ab} denote the electromagnetic field-tensor, and $BdA = F_{ab}dx^a dx^b$ describe the magnetic field B . B counts the number of magnetic field-lines per unit surface area dA of surface elements $dx^a dx^b$, properly measured by observers with world-lines orthogonal to dA [75]. Then

$$\partial_t \rightarrow \partial_t + \mathcal{L}_\omega \quad (18)$$

applied to B gives a net time-rate of change as seen by distant, nonrotating observers. Here, the Lie derivative \mathcal{L}_ω generalizes the Lagrangian derivative, by including the coordinate transformation to the nonrotating Boyer-Lindquist coordinates (e.g. [72]). The induced electric field E' thus observed by Faraday's law now includes an additional term [75]

$$\nabla \times E' = -\partial_t B + 4\pi \mathcal{J}_m, \quad (19)$$

here expressed as a current

$$\mathcal{J}_m = \frac{1}{4\pi} \mathcal{L}_\omega B \quad (20)$$

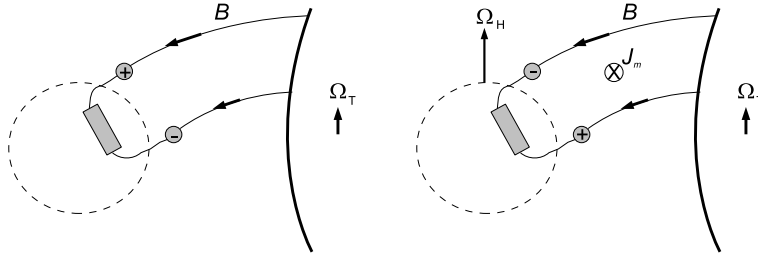


Fig. 2 Shown is a schematic of the action of black hole spin onto a surrounding torus magnetosphere, supported by a uniformly magnetized torus. Faraday induction acts on rigidly rotating, force-free magnetic field-lines of an inner torus magnetosphere with no-slip boundary conditions on the inner face of a torus with angular velocity Ω_T , here around a Schwarzschild black hole (*left*) and around a rapidly rotating Kerr black hole (*right*) whose angular velocity Ω_H exceeds Ω_T . Note the sign change in the induced electric polarization at the terminals, as seen in the non-rotating Boyer-Lindquist coordinate frame. The result can be attributed to an EMF induced by frame-dragging, here expressed in terms of the current $\mathcal{J}_m = \frac{1}{4\pi} \mathcal{L}_\omega B$. The EMF produces a poloidal current upon closure over the horizon surface, given its finite surface impedance ([75], indicated by the resistor element) by the no-hair theorem, and hence Maxwell stresses on the event horizon [69] and the inner face of the torus [79].

of virtual magnetic monopoles. It renders explicit the generation of an EMF by frame-dragging, illustrated in Fig.(2).

Magnetic flux-surfaces, with no-slip boundary conditions on the inner face of the torus, like those on the surface of the Sun, can extend towards the event horizon as rigid wires in the force-free approximation [75]. The EMF induced by \mathcal{J}_m (19) induces an electric current upon connection to the event horizon, facilitated by maximal flux supported by the equilibrium magnetic moment of the black hole, by current closure over the finite horizon impedance equal to that of radiative infinity [75]. Thus, an inner torus magnetosphere mediates Maxwell stresses on the event horizon [69] and Maxwell stresses on the inner face of the torus [79], producing a transfer of energy and angular momentum between the black hole and the torus described by (22). It will be appreciated that the horizon surface hereby forms a passive load. Current closure over the horizon and its finite impedance can be attributed to the no-hair theorem, described intuitively in terms of the membrane paradigm of [75].

The details of inflowing plasma has been a topic of considerable discussions in the literature (see [47] and references therein), which, however, falls outside the scope of the present discussion. We limit our discussion to frame-dragging as the underlying causal agent for the interaction with the torus magnetosphere, here expressed by \mathcal{J}_m .

The equivalence between spin-up of a torus by radiation onto a rapidly spinning black hole and spin-down of a pulsar by radiation to infinity leads to catalytic conversion of black hole spin energy. With no small geometrical parameter present in the inner torus magnetosphere it represents the dominant radiative process, thus setting the evolution and lifetime of black hole spin. In this *closed model approximation*, the accompanying torque T and black hole luminosity L_H mediated by the inner torus magnetosphere satisfy [79]

$$T = -\dot{J}, \quad L_H = -\dot{M}, \quad (21)$$

giving rise to suspended accretion [81] described by

$$\begin{cases} \dot{M} = -e\Omega_H(1-\eta)\Omega_T \\ \dot{J} = -e\Omega_H(1-\eta) \end{cases}, \quad (22)$$

where

$$\eta = \frac{\Omega_T}{\Omega_H} \quad (23)$$

denotes the angular velocity of the torus relative to that of the black hole and e represents the strength of inner torus magnetosphere. Here, the coupling between the inner and outer faces of the torus is mediated by a flat infrared spectrum in magnetohydrodynamical turbulence [82, 93]. (The associated Reynolds number is large, e.g., $\text{Re} = \mathcal{E}_k / \mathcal{E}_d \sim 10^8 M_9^{-1}$, where \mathcal{E}_d refers to the product of dissipation by turbulent MHD stresses times the Alfvén crossing time of the disk.) In (22), we

neglect the sub-dominant energetic output along open magnetic flux-tubes along the spin-axis of §2.2. While the angular velocity Ω_T is will not be equal to the angular velocity Ω_{ISCO} at the inner most stable circular orbit (ISCO), especially at maximal spin-rates of the black hole, Ω_T and Ω_{ISCO} will be tightly correlated and more so, as the ISCO expands [79]. This closure condition allows (22) to be integrated directly for various initial conditions of the black hole parameters. Integrations of modified equations of suspended accretion that include precession have also been performed [44].

At the threshold of magnetic stability (5), the lifetime of spin is correlated to the mass of the inner disk according to [88]

$$M_D \simeq 120M_\odot \left(\frac{\mathcal{E}_k}{15\mathcal{E}_B} \right) \left(\frac{R_D}{6R_g} \right)^4 \left(\frac{M_9^2}{T_7} \right), \quad (24)$$

$$M_D \simeq 0.1M_\odot \left(\frac{\mathcal{E}_k}{15\mathcal{E}_B} \right) \left(\frac{R_D}{6R_g} \right)^4 \left(\frac{M}{7M_\odot} \right)^2 \left(\frac{20\text{s}}{T_{90}} \right), \quad (25)$$

with characteristic densities of $7.9 \times 10^{-11} \text{ g cm}^{-3}$ and, respectively, $1.9 \times 10^{11} \text{ g cm}^{-3}$ (close to the neutron drip line) and very similar Alfvén velocities $v_A = 0.1052c$ and, respectively, $v_A = 0.1072c$, where c denotes the velocity of light.

4 UHECRs from linear acceleration of ionic contaminants

The induction potentials of supermassive black holes surrounded by magnetic fields have been previously recognized for their ability to create UHECRs in dormant AGN, such as remnants quasars, to facilitate their escape to infinity [14]. If produced in the proximity of the black hole, then there are strict conditions for UHECRs to escape to infinity, by exposure to curvature radiation drag, which may limit their energies to the TeV range [45], inverse Compton scattering on radiation from the accretion disk and photon-pion absorption of UHECRs [47, 48]. At the same time, there are minimum requirements on the activity of a nucleus to produce energies in the range of the GZK threshold [95]. The latter represents conditions for instantaneous production of UHECRs and should not be viewed as a restriction on the mean activity [24, 89], since the latter depends on the duty cycle of the source [78].

The recent Pierre Auger Observatory provides the first hint at a correlation between UHECRs above the Greisen-Zatsepin-Kuzmin (GZK) [35, 97] threshold of $5.6 \times 10^{19} \text{ eV}$ with nearby AGN listed in the Véron-Cetty and Véron catalogue [91], up to a distance of 75 Mpc. The physical association of UHECRs with AGN remains tentative, awaiting improved statistics with a larger number of detections of events, currently approaching one hundred. Nevertheless, the association with AGN is attractive. The typical dimensions of the nuclei, i.e., the central black hole and a surrounding ion torus, on the order of ten light years points to a correspond-

ing large-scale ordered electric field of merely 6.6 V/cm for protons at the GZK threshold energy.

The linear accelerator upstream of an outgoing Alfvén front, ahead of a leptonic outflow by the relativistic capillary effect of §2.2, is an attractive site for producing UHECRs from ion contaminants at energies close to the Fermi-level of the central supermassive black hole. Fig.(3) illustrates the pick-up of ionic contaminants, by UV irradiation coming off an ion torus, that have linear sizes typically on the order of light years (60 light years in the FR I M87 [25]; it has been noted that M87 is not seen as a source of UHECRs by the PAO, however). At appreciable distances away from the central black hole, this linear accelerator is unlikely to be limited by curvature radiation. This possibility appears to be overlooked in previous discussions [58].

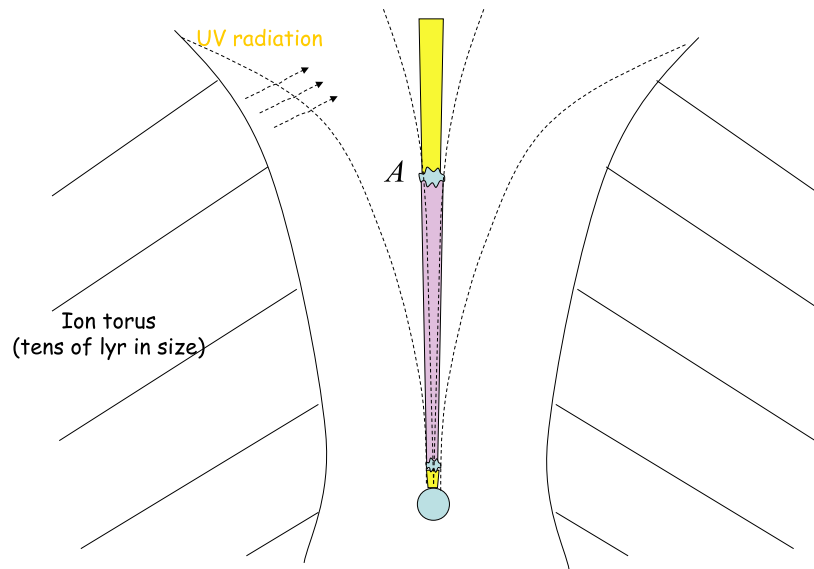


Fig. 3 A Faraday-induced horizon Fermi-level [80] is mediated to large distances by the extraction of a leptonic outflow along equipotential magnetic flux-surfaces by a relativistic capillary effect. This outflow terminates in an outgoing Alfvén front *A*. Upstream of *A*, the magnetic flux-surfaces are essentially charge free, and stable against pair-cascade at large distances from the black hole. (Frame-dragging rapidly decays with the cube of the distance from the black hole.) Here, ions are produced from stray particles by exposure from UV-radiation from an ion torus, whose linear size is typically on the order of ten light-years in AGN. These ion contaminants are subject to linear acceleration by the generating voltages at the Alfvén surface, which increase with poloidal angle away from the polar axis. In this process, the black hole spin-down against the inner disk is via an inner torus magnetosphere (not shown) equivalent in poloidal topology to pulsar magnetospheres, discussed in §2.3. (Reprinted from [88])

A test comes from a correlation between the UHECR energies and the observable mass and lifetime of the black hole. Casting (6) in dimensionful form, the model can be tested observationally, by way of the correlation function [88]

$$\mathcal{E} = 5.6 \times 10^{19} \sqrt{\frac{M_9}{T_7}} \left(\frac{\theta_H}{0.5} \right)^2 \text{ eV} \quad (26)$$

where we take the observed opening angle of 60° in M87 as a fiducial value ($\theta_H = 0.5$ rad [40]). In (26), we have expressed the underlying poloidal magnetic field-energy – which is difficult to observe directly – with the finite lifetime of rapid spin of the black hole. It can be associated with the lifetime of the AGN, which is typically on the order of millions of years. We mention the 1-10 Myr lifetimes of the radio-loud Fanaroff-Riley II sources [59], although these sources are not the focal point of (26). For typical ages of AGN, the correlation function (26) is in excellent agreement with the PAO observations.

The correlation (26) should be viewed in a time-dependent context, in response to intermittent activity with low duty-cycle of the central black hole, e.g., by variability in accretion or instabilities in the inner torus magnetosphere surrounding the black hole. Intermittencies in the inner disk, as in MCG 60-30-15 [74], inevitably modulate the half-opening angle $\theta_H(t)$ in time and, thereby, the instantaneous luminosity in the jet [88]

$$L_j(t) \simeq 1.3 \times 10^{46} \left(\frac{M_9}{T_7} \right) \left(\frac{\theta_H(t)}{0.5} \right)^4 \text{ erg s}^{-1} \quad (27)$$

up to several orders of magnitude. Thus, UHECRs with energies (26) can be viewed as “sparks” in intermittent AGN of otherwise low average luminosity (small $< \theta_H^4(t) >$). This possibly applies to Seyfert galaxies and LINERs seen in the present tentative association of UHECRs with nearby AGN [56], consistent with their ability to escape of infinity. It would therefore be of interest to address more specifically the ages of Seyfert galaxies and long-term monitoring of the inner disk radius by X-ray spectroscopy, for a quantitative observational test of (26).

5 GRBs from leptonic outflows extracted by a capillary effect

HETE II and Swift observations reveal long GRBs with and without supernovae, and a diversity in their X-ray afterglow emissions. This is consistent with a diversity in the origin of long GRBs with otherwise a common inner engine. The durations of tens of seconds, therefore, are to be viewed as intrinsic to the inner engine. The gamma-ray emission process does not, by itself, account for long durations, as can be inferred from short-variability [66] and the existence of both short and long GRBs in the BATSE catalogue.

Here, we identify the long durations with the lifetime of rapid spin of a stellar mass black hole in suspended accretion. The durations of tens of seconds are recovered in interactions with tori of up to about 0.1 solar mass of high-density matter, as expressed in (25). This applies naturally to newly born black holes, as in a core-collapse of massive stars or the merger and tidal break-up of a neutron star with another neutron star or companion black holes, in case the latter rotates rapidly.

The evolution equations (22) predict an exponential decay in the relaxation of a rapidly rotating black hole to a slowly rotating nearly Schwarzschild black hole. We recently searched for the presence of such viscous behavior in light-curves of long GRBs by matched filtering of these light curves against the theoretical template produced by (22) [88]. Our model Kerr-template follows by integration of (22) for a black hole with initially maximal spin. The minor energy output in gamma-rays is calculated on the basis of (22), by positing a positive correlation between the ISCO

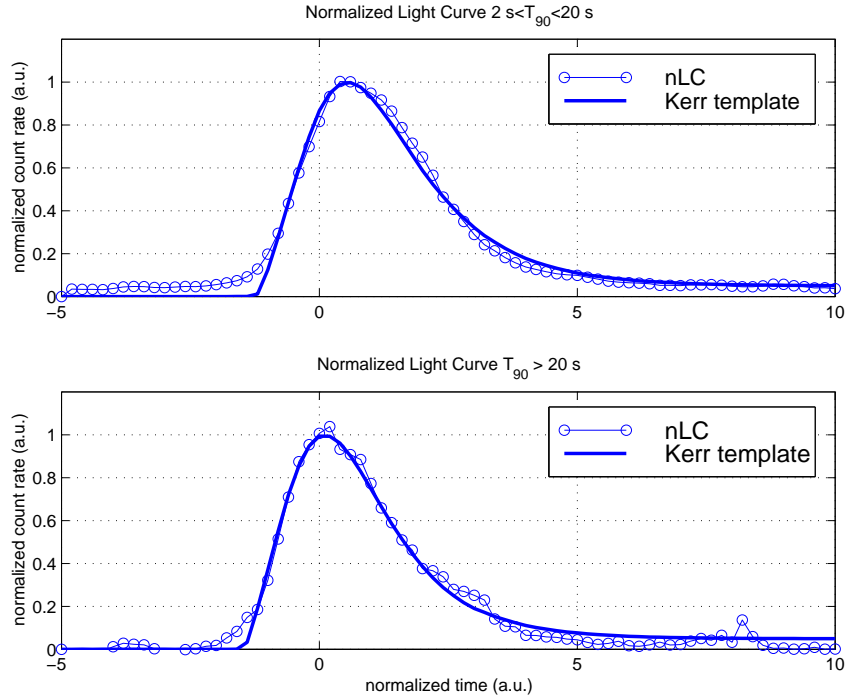


Fig. 4 Shown is the normalized light curve (nLC) representing the ensemble average of long-duration BATSE light curves based on averaging 300 blindly selected long events in sample L1: $2 \text{ s} < T_{90} < 20 \text{ s}$ (*top*) and 300 blindly selected long events in L2: $T_{90} > 20 \text{ s}$ (*below*) in the BATSE catalogue. Here, T_{90} is the duration representing 90% of the burst emission received in the BATSE detectors. Evidently, convergence of the averaging process is slower in L2 than in L1, which may be attributed to frequent intermediate periods of quiescence. The results show excellent agreement with viscous spin-down of a Kerr black hole. Furthermore, the match to the Kerr template appears to be best for L2, which is consistent with the longest duration GRBs being produced by nearly extremal black holes. (*Reprinted from* [88])

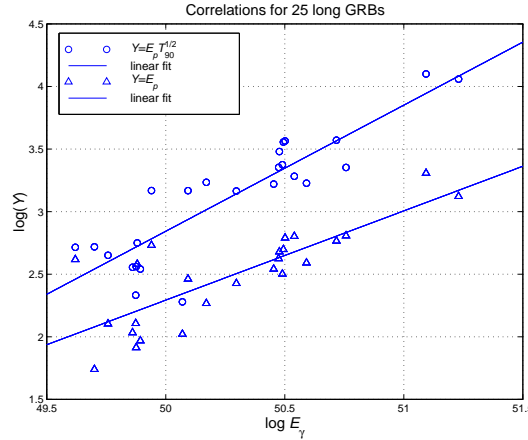


Fig. 5 Shown is the correlation in the published data of [4, 30, 31] between the peak energy E_p , the true energy E_γ in γ -rays of long-duration GRBs with known redshifts and inferred opening angles, assuming a stellar-wind type environment to the gamma-ray burst progenitor and using redshift corrected durations T_{90} . A linear fit gives a slope and Pearson coefficient $(s, c) = (1.01, 0.85)$ to $Y = \log(E_p T_{90}^{1/2})$ (circles) and $(s, c) = (0.71, 0.76)$ in the Ghirlanda correlation to $Y = \log(E_p)$ (triangles). (Reprinted from [80])

and the half-opening angle of the open magnetic flux-tube on the event horizon of the black hole [88]. The open outflows hereby gradually open up as the black hole begins to spin down, marked by a slow rise in high-energy emissions whenever the black hole is initially at near-maximal spin.

Our matched filtering begins with normalizing the light curves in the BATSE catalogue in durations and count-rates by optimal fit to the model Kerr template. This is a three parameter fit, including the time-of-onset. These normalized results can be summed directly for averaging. In this process, all short timescale fluctuations are filtered out, such as short and intermediate timescale fluctuations due to shocks and instabilities in the vicinity of the black hole (the inner torus magnetosphere and the torus itself) and orientation effects by jets and disks. Fig.(4) shows that matched filtering of the GRB light curves against a Kerr template. The results are remarkably consistent with a process of viscous spin-down of Kerr black holes. It suggests the creation of astronomical amounts of Bekenstein-Hawking entropy in the event horizon, at least 40% of the initial spin-energy, while at most 60% is radiated off to infinity by the torus in various radiation channels. It gives rise to a spectral-energy correlation which takes into account the finite lifetime of black hole spin (Fig.5).

Following §2.2, the GRB-afterglow emissions represent the dissipation of kinetic energy in the leptonic outflow extracted by the capillary effect, here in internal and external shocks [68]. Let c_1 denote the ratio of observed peak energy E_p to \mathcal{E} . It comprises the combined efficiency of converting \mathcal{E} into kinetic energy in a neutron-enriched leptonic jet with subsequent conversion into high-energy gamma-rays in shocks. The luminosity in Poynting flux along the open magnetic flux-tube in the

force-free limit [33, 13, 75] is $L = \Omega_A^2 A_\phi^2$. Let c_2 denote the efficiency of converting L into the true energy in γ -rays: $E_\gamma = c_2 L T_{90}$. Then (6) predicts $E_p T_{90}^{1/2} = ekE_\gamma^{1/2}$, where $k = 2c_1/\sqrt{c_2}$. In the approximation of commensurate angular velocities, i.e., Ω_F, ω to be of order Ω_H , the Ghirlanda relation [30] $E_p \propto E_\gamma^{0.7}$, and the Eichler & Jontof-Hutter correlation between E_p and kinetic energy of the outflow [21] $c_1 \propto E_p^{3/2}$ gives $k \propto E_\gamma^{21/40} \simeq E_\gamma^{1/2}$, so that

$$E_p T_{90}^{1/2} \propto E_\gamma, \quad (28)$$

where the observed values of E_γ show a narrow distribution around 10^{51} erg [26]). Fig.5 shows the correlation (28) in a compilation of HETE II and Swift data [4, 30, 31]. See also [30] for an alternative perspective on the basis of viewing angles.

6 Unification of nonthermal transient sources

With or without spin, black holes offer unique sites for powerful energetic processes in the Transient Universe with considerable potential for unification, essentially parametrized by the black hole mass and lifetime of its spin in correlation to the physical properties of the surrounding disk. A long-standing open question is whether a source is accretion powered or spin-powered. The total luminosity is important criterion in observational classification schemes. It is, however, insufficient to identify black hole spin [50]. Here, we focus on cases when black hole spin is important, even when not necessarily dominant in total energetics.

6.1 UHECRs from low-luminosity, intermittent AGN

The PAO identification of UHECR with sources nearby, in angular correlation to some of the nearby galaxies has raised a number of questions.

Based on the all Sky Survey (HIPASS), some authors [32] find that the PAO detections of UHECRs above the GZK threshold are related to spiral galaxies. This could include contributions from stellar mass transients, but does not rule out the activity of dormant AGN [46], nor does it account for the paucity of UHECRs in the Virgo cluster [98]. Extended with the NASA/IPAC Extragalactic Database (NED), the UHECRs detected by the PAO appear to be associated with low-luminosity Seyfert galaxies and Low-Ionization Nuclear Emission Line Regions (LINERs) with relatively few radio galaxies [56]. There is no indication of an association with BL Lac objects [37] and there might exist a minimum bolometric luminosity for the production of UHECRs to unsue, consistent with the paucity of UHECRs from the Virgo cluster [98].

Proposed associations of UHECRs with radio-galaxies [57] include diffusive acceleration of charged particles in radio lobes [28]. If so, this would require the radio-jet to be baryon-rich, to account for the observed broad mass-range of the UHECR hadrons. It would not account for UHECRs associated with the above-mentioned Seyfert galaxies and LINERs [56].

In §2.2, a mechanism of linear acceleration is described for intermittent AGN with low average luminosities. If this association is confirmed by improved statistics of the PAO, then UHECR-AGN and UHECR-inactive AGN provide important information for unification of the diverse AGN Zoology, further combining black hole mass and spin, the state of matter of their surrounding disks or tori and the observer's viewing angle [5, 77, 39]. A rather clear dichotomy appears notably in

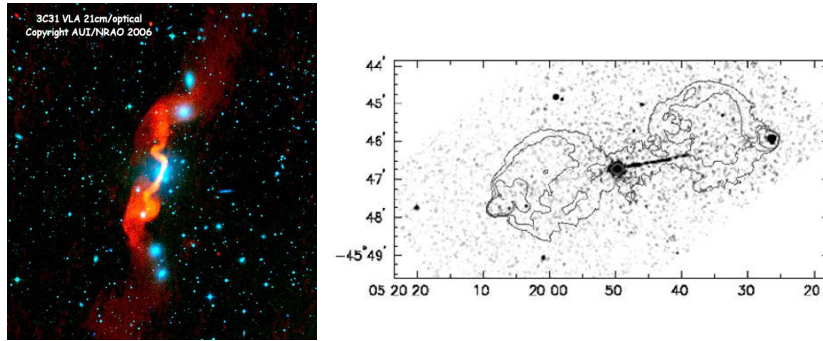


Fig. 6 The extragalactic radio-sources 3C31 (NRAO/AUI/NSF) and Pictor A (NRAO/AUI/NSF) exemplify AGN of type Fanaroff-Riley I and II. The latter are considerably more powerful, display straight (orientation stable) one-sided jets and are lobe-dominated in their synchrotron radiation output. A somewhat similar dichotomy can be found in galactic transients, such as SS433 [54] and the micro-quasars GRS 1915+105 [55], both harboring stellar mass black holes.

radio-galaxies. Fanaroff & Riley [23] identify AGN of Type I and II, such as, respectively, 3C31 and Pic A shown in Fig. 6, featuring the morphological distinctions in radio galaxies: FR II sources are lobe-dominated and edge-brightened, straight and one-sided, which is testimony to their power, exceptional long-term orientation stability and beaming in relativistic outflows. A somewhat similar morphological dichotomy can be found in stellar mass transient sources, notably the black hole candidate sources SS433 and GRS 1915+105, featuring outflows with velocities of 0.29 and 0.92 times the velocity of light, respectively. It should be mentioned that both are highly non-trivial sources in many ways, e.g., SS433 shows line-spectra reflecting baryon-rich outflows, while GRS 1915+105 is featureless and highly intermittent.

Can the large-scale FR I and FR II dichotomy can be put into context with black hole accretion versus black hole spin-powered systems [8]? This will be difficult to address with any certainty, without more direct probes of the physics of the innermost regions of the AGN, e.g., in the X-rays [74] or low-frequency gravitational-waves produced in so-called extreme mass-ratio inspirals of stellar mass objects

captured by the central supermassive black hole (EMRIs, these Proceedings), or during exceptional events such as the merger of a binary of two supermassive black holes.

If the majority of the UHECRs beyond the GZK threshold detected by the PAO are produced by AGN, then the association to radio-quiet Seyfert galaxies and LINERs is remarkable. It is tempting to associate UHECR-AGN with supermassive black holes with spin and variable inner disks, such as the Seyfert galaxy MCG 60-30-15 [74], with possibly low duty cycle of activity. The proposed linear acceleration upstream an Alfvén front would then naturally account for an output in UHECRs. It also poses the question, how spinning black holes in Seyfert nuclei would remain sub-luminous in the radio, while those in FR II galaxies are radio-loud.

One possibility might be suppression of radio-jets due to the absence of disk winds, perhaps due to weak poloidal magnetic fields[88]. (When jets do form, polarization studies on FR I and II jets show large-scale ordered magnetic fields, with different orientations relative to the axis of the jet.) Black hole spin interacts largely with the inner disk or inner face of a surrounding torus, through the time-average energy density of net flux in the poloidal magnetic field. The black hole remains energetically active even when the $m = 0$ component of the magnetic field remains strongly intermittent. If outer disk winds are suppressed by turbulence (even as the inner disk receives power from the black hole [79]), the jets that form will be largely leptonic in the form of black hole outflows only. (cf. the jet X-ray jet of the Crab pulsar [52].) Without baryonic contaminants, these outflows probably do not form sites of re-acceleration of charged particles, as in shocks (cf. modeling GRB-afterglows from baryon-poor jets [68]), and hence be weak or unseen in extended radio-emissions. It would be of interest to study this picture in more detail, to see if it can account for UHECRs from the active nuclei of Seyferts and LINERs.

Another possibility is pointed out in our Outlook below.

6.2 Long and short GRBs from rotating black holes

Cosmological gamma-ray bursts come in at least two varieties: short bursts of tenths of seconds and long bursts of tens of seconds, shown in Fig.(7). Modeling GRBs from rotating black holes naturally accounts for these two durations, by positing slowly and rapidly rotating black holes in a state of hyperaccretion and, respectively, suspended accretion. With a common physical mechanism for producing nonthermal emissions directly by the spinning black hole (6). This predicts (weak) X-ray afterglows also from short bursts[81], confirmed by the Swift event 050509B [29] and the HETE II event 050709 [92].

Notably, the true energy in gamma-rays from long GRBs [26] is a small fraction of the spin energy of a rotating stellar mass black hole, in quantitative agreement with with the sub-dominant output along the spin-axis over the course of spin-down against a surrounding torus [83].

The non-uniform horizon Fermi-level $\nu_F(\theta)$ (Table I) gives rise to non-uniform leptonic outflows by (6), whose intensity increases with the angle of the magnetic flux-tubes relative to the spin-axis of the black hole. It is formally zero on-axis. Conceivably, variability also reaches a maximum in a boundary layer with the surrounding baryon-rich torus winds. If so, variability and luminosity depends on the viewing angle (in light of relativistic beaming effects) and can explain the observed correlation between variability and luminosity [67]. In the nLC, this orientation effect is effectively averaged out, whereas for an individual burst when seen along the edge of its conical outflow, a highly variable GRB light-curve may be accompanied by an exceptionally powerful optical afterglow, such as GRB 080319B [62].

Gamma-ray emissions from leptonic outflows powered by (6) arise naturally from rapidly spinning black holes formed in collapsars[96, 85], as well as mergers of a neutron star with another neutron star [12] or with a rapidly spinning, companion black hole [60, 79], illustrated in Fig.(8). As a common inner engine, it can explain the HETE II event GRB 030329/SN2003dh and the Swift event GRB060614 without a supernova, and a diversity in X-ray afterglows, indicative of the host environment. For example, it can explain the long-durations in GRB 050911 [61], which appeared to have taken place in a low-density environment typical for binaries of stellar remnants.

For long GRBs from collapsars, fall-back of the remnant stellar envelope can account for the long-lasting X-ray plateau's discovered by Swift in GRB-supernovae

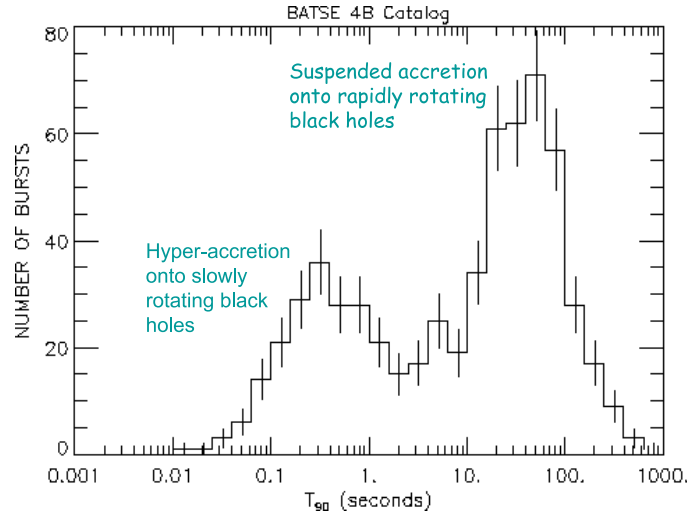


Fig. 7 The BATSE catalogue reveals a bimodal distribution of durations in gamma-ray bursts, of short bursts of tenths of seconds and long bursts of tens of seconds. These durations agree with hyper- and suspended accretion onto slowly and, respectively, rapidly rotating black holes, whose initial angular velocities satisfy $\Omega_H < \Omega_T$ and, respectively, $\Omega_H > \Omega_T$. It predicts (weak) X-ray afterglows also to short bursts, confirmed by HETE II and Swift in 2005. (Courtesy of NASA Marschall Space Flight Center, Space Sciences Laboratory.)

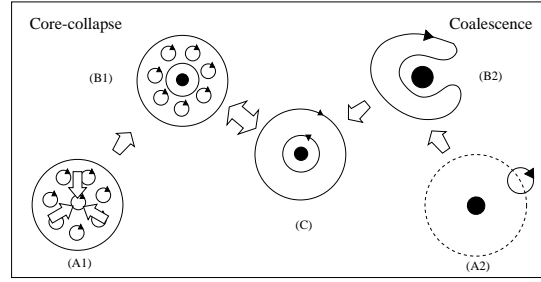


Fig. 8 Rotating black holes surrounded by high-density matter form a common endpoint in collapsars (A1-B1-C, *left*) and the merger of a neutron star around a black hole (A2-B2-C, *right*), where rotation of the latter facilitates tidal break-up outside the ISCO. The same endpoint (C) appears in numerical simulations of the coalescence of two neutron stars [12]. As a common inner engine, it naturally accounts for long GRBs with and without supernovae and a diversity in their X-ray afterglow emissions. (Reprinted from [83].)

[43]. In our model, it would commence *after* black hole spin-down, subsequent to a sudden transition from suspended to hyperaccretion onto a slowly spinning black hole. In contrast, mergers of neutron stars with another neutron star or a rapidly spinning black hole companion suggests a strongly reduced X-ray plateau, as in GRB060614 and GRB050911 versus GRB070110 [76] or GRB 030329/SN2003dh, consistent with low-density host environments of some of the long GRBs, different from a progenitor stellar wind decay of r^{-2} .

The explosion mechanism in collapsar events appears to receive a substantial input from an angular momentum-powered inner engine, inferred from highly aspherical expansion [38]. This can be expected to arise by aspherical irradiation from within by magnetic disk winds [83]. In collapsars, the newly formed black holes are not without kick. Only those with sufficiently small kick velocities does remain centered. The fraction of collapsars thus producing a long GRB is hereby small. An estimate based on the Bekenstein gravitational-radiation recoil mechanism [9] shows that this fraction is consistent with the observed branching ratio of about 0.2-0.4% of the SN Type Ib/c producing GRBs [85].

Accretion-powered models (e.g [96, 43]) are different. The burst durations are determined by the timescale of matter infall, e.g., from a remnant stellar envelope. As such, they do not account for GRB060614, as it was not a core-collapse event [19]. Winds from the inner disk, at typical temperatures of 1-2 MeV, are too contaminated to produce ultra-relativistic (baryon-poor) outflows as input to the observed GRB-afterglow emissions. If attributed to the central black hole, then spin *up* by accretion [43] is at odds with the decay in the normalized ensemble average of BATSE light curves (Fig. 4). More generally, accretion powered models are *open models* with outflows along the spin-axis of the black hole representing a major fraction of the black hole output ([13], developed for slowly spinning black holes with $Q = 0$, and [70, 53]). Long GRBs representing a substantial fraction of black hole spin-energy is ruled out by the existing statistics on the true energy in gamma-rays [26].

7 Conclusions and Outlook

Perhaps the most exciting prospect of Kerr black holes is a unification of some of the most exceptional nonthermal events in the Transient Universe. At present, our focus is on UHECRs and cosmological gamma-ray bursts, where we find good agreement with current observations. In the future, this may extend to high-energy neutrinos, radio, as in a report on a short extragalactic radio burst [51], and gravitational-wave emissions [6]. Ultimately, these channels promise an ever-more detailed picture of the “physics of nonthermal radiation” at work in these enigmatic sources, especially how this relates to the state of matter surrounding the black hole.

Key questions in transient sources from rotating black holes, is whether they are accretion- or spin-powered, and how to account for their durations, energy output into various emission channels, spectral-energy correlations, light curves and luminosities.

Here, we describe a model for concurrent nonthermal transient emissions in ionic contaminants and high-energy photons, associated with a linear accelerator ahead of a leptonic or baryon-poor jet. The jet is produced by a relativistic capillary effect, and terminates in an Alfvén front that communicates the horizon Fermi-level out to large distances. The jet forms a finite junction (bounded by Alfvén fronts) between the event horizon of the black hole and infinity, in response to their relative angular velocities and reflection-symmetric radiation boundary conditions. The outgoing Alfvén front is hereby representative for the raw Faraday-induced induction potential of the black hole whereby, somewhat ironically, it opens the way to producing UHECRs ahead of lower-energy photon emissions. Quite generally, therefore, one expects a diversity in nonthermal high-energy emissions in hadrons and photons, whereby the observed spectrum will be largely determined by absorption and/or obscuration associated with the specific nucleus and host environment.

For UHECRs, there is tentative evidence for a correlation of UHECRs with low-luminosity Seyfert galaxies and LINERS. For GRBs, there is, in addition to a bimodal distribution of durations, increasing quantitative phenomenology on their origin – with and without supernovae – and host environments given a diversity in X-ray afterglows.

We attribute UHECR-AGN to linear acceleration of ion contaminants with intermittent and on-average low-luminosity activity of a supermassive spinning black hole described in (26-27). Our model correlation function between energies and the mass of the black hole in agreement with the GZK threshold, when associating the lifetime of black hole spin with that of AGN. This approach is consistent with UHECRs from nearby Seyfert and LINERs, as suggested by the recent PAO results. Here, the Seyfert galaxies may well host supermassive spinning black holes with intermittent activity in its inner disk, as in the Seyfert galaxies MCG 60-30-15. The proposed linear acceleration upstream of an outgoing Alfvén front at large distances away from the central black hole solves two challenges: it circumvents limiting curvature radiation and it allows UHECRs to escape from nuclei that are not necessarily dormant (but otherwise of low average luminosity).

In our model, the production of UHECRs is naturally accompanied by high-energy photon emissions in the underlying baryon-poor jet. On this basis, one expects UHECR-AGN to produce, intermittently, a low-luminosity output in Very High Energy (VHE) gamma-rays. However, both UHECR- and VHE-emissions will be highly beamed, possibly with different beaming factors, so that concurrent detections could be rare. Cen A appears to be a source that radiates in both these channels [3]. Yet, most TeV-AGN are BL Lac sources [49], while no BL Lac are UHECR-AGN in the present PAO sample [37]. Combined surveys of UHECRs and VHE gamma-rays promise to be instrumental in resolving these puzzles and their relation to the type of AGN, possibly including their relevance to Seyfert galaxies.

We identify long GRBs with nearly complete spin-down of rapidly rotating stellar mass black holes against surrounding high-density matter. It represents a common inner engine, and accounts for:

- long-durations of tens of seconds of the lifetime of spin of black holes in collapsars and mergers, of neutron stars with another neutron star or a companion black hole (Fig.8), explaining events with and without supernovae and a diversity in X-ray afterglows,
- true energies in gamma-rays representing a minor release of spin-energy [83] consistent with the observed statistics [26],
- a model spectral-energy correlation (28) in agreement with HETE II and Swift data, shown in Fig.(5),
- an exponential decay in the intrinsic light curves of long GRBs defined by the average of 600 light curves, in agreement with the model template shown in Fig.(4).

We conclude that long GRBs are spin-powered in suspended accretion, not accretion-powered.

Following §6.2, we attribute short GRBs to similar high-energy emissions from slowly rotating black holes in a short-duration episode of hyper-accretion. This predicts (weak) X-ray afterglows also to short GRBs [81], confirmed in 2005 by HETE II and Swift.

7.1 Gravitational radiation from turbulent flows around black holes

Turbulence appears to be inevitable in flows around black holes. To be sure, they bring along multipole mass-moments (which sets it apart from Taylor-Couette flows in existing laboratory experiments), that are luminous in gravitational radiation with frequencies on the order of 1 kHz around stellar mass black holes and below 1 mHz around supermassive black holes. It might already have been seen in some of the recently discovered quasi-period oscillations around supermassive black holes [34, 36]. One of the most exciting prospects for astronomy in the present century is to directly “listen into” these turbulent flows in close proximity to an event horizon by

upcoming gravitational-wave experiments. Any such detection promises to identify physical properties that hitherto remain outside the realm of direct measurements, such as magnetic fields, presently resolved at about one-thousand Schwarzschild radii in selected AGN, the effective viscosity, structure and stability of the inner disk and the inner torus magnetosphere, magnetic disk winds and, ultimately, metrology on the central black hole itself.

An outlook on this scientific opportunity is the following.

Gravitational waves are the dominant radiation channel for a strong coupling between the inner and outer face of the torus, and appear to be mostly in quadrupole emissions [15]. An equipartition $\delta m/M_D \simeq \mathcal{E}_B/\mathcal{E}_k \simeq 1/15$ of the quadrupole mass inhomogeneity δm points to quasi-periodic, broad-line gravitational radiation with a luminosity

$$L_{GW} = \frac{32c^5}{5G} \left(\frac{M_H}{R_D}\right)^5 \left(\frac{\delta M_2}{M}\right)^2 = 7 \times 10^{41} \left(\frac{R_D}{6M}\right)^3 \left(\frac{M_9}{T_7}\right)^2 \text{ erg s}^{-1}, \quad (29)$$

with frequencies

$$f_{gw} = 5M_{H,6}^{-1} \frac{6.2}{(R_D/M_H)^{3/2} + (a/M_H)} \text{ mHz} \quad (30)$$

corresponding to the band width of sensitivity of the planned LISA mission. Emissions that extend over a finite bandwidth $B = 0.1 \times B_{0.1}$ at from a source at distance D , integration of L_{GW} over a time t_1 in units of years gives a characteristic strain amplitude

$$h_{char} = \frac{\sqrt{2}}{\pi D} \sqrt{\frac{dE}{df}} = 1 \times 10^{-21} D_{100}^{-1} B_{0.1}^{-1/2} \left(\frac{R_D}{3M_{H,9}}\right)^{3/2} \left(\frac{M_{H,9}}{T_7}\right) t_1^{1/2} \quad (31)$$

where we ignored a redshift factor $1+z$ for the nearby source AGN of interest. For SgrA*, this h_{char} might strike the threshold of sensitivity of LISA, depending on the approximations used, but most likely remains undetectable for extragalactic nuclei, as illustrated in Fig.(9). If detected, LISA will open a unique window to studying high-Reynolds number turbulence around a supermassive black hole.

For stellar mass black holes powering long GRBs, the gravitational-wave emissions will be detectable by Advanced LIGO-Virgo within a distance of about 100 Mpc, corresponding to one long GRB per year. Detection of the light curve in gravitational radiation is of interest, as it features a *negative chirp* associated with the expansion of the ISCO, during relaxation of the Kerr spacetime to a nearly Schwarzschild spacetime. The late-time frequency of gravitational-wave emissions provides novel metrology of the mass of the black hole, according to

$$M \simeq 5.9 \left(\frac{f_{GW}}{1 \text{ kHz}}\right)^{-1} M_{\odot}. \quad (32)$$

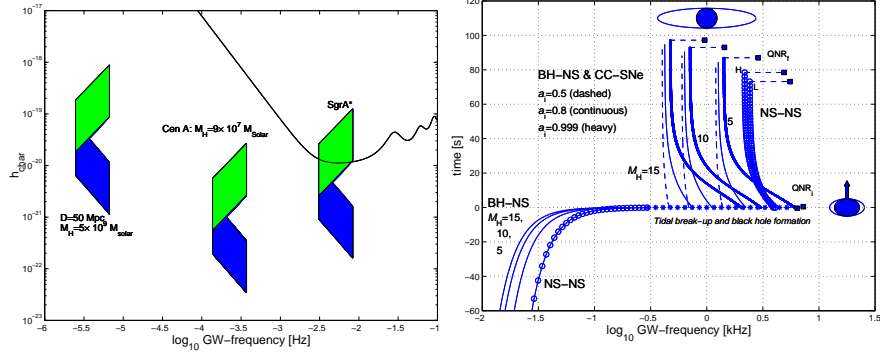


Fig. 9 (*Left.*) Shown are estimates of the gravitational-wave signals from forced turbulence in accretion disks around supermassive black holes with rapid spin, including the strain-amplitude noise curve of a typical LISA configuration (continuous line). The source amplitudes refer to a one-year integration time of quasi-periodic oscillations produced by quadrupole moments in the inner disk with an assumed 1% line-width, calculated for the entire evolution of spin over $T = 10^6$ yr and $T = 10^7$ yr. The blue parallelograms refer conservatively to co-evolution of disk mass, whereas the green parallelograms refer to a constant disk mass. The quadrupole mass-moment is coupled to the multi-pole moments in the magnetic field in the fully turbulent flows. SgrA* appears to be a candidate source of some interest, while extragalactic AGN appear to be out of reach. (*Right.*) An overview of the diversity in origins of long GRBs, here in terms of chirps in gravitational radiation. The third quadrant shows positive chirps, produced by coalescence of neutron stars with another neutron star or a rapidly rotating companion black hole, while the first quadrant shows negative chirps produced post-coalescence or in collapsars during viscous spin-down of a rapidly rotating stellar mass black hole. In case of mergers, the naked inner engine may also be observable as a radio burst for tens of seconds. Combined LIGO-Virgo/LOFAR observations promise complete identification of the mysterious common inner engine to long GRBs. (Reprinted from [89].)

In the coming years, improved statistics of the PAO will clarify the association with nearby AGN. If true, UHECR-AGN will be an important augmentation to the AGN Zoology. A direct probe of motions in the inner disk of AGN by LISA appears to be limited to SgrA*, shown in Fig.(9). Its gravitational-wave emissions may represent most of its energy output. If UHECR-AGN are loud in gravitational radiation, then these unseen emissions could account for their low luminosities in the electromagnetic spectrum. Scaled to high-density tori around stellar mass black holes in collapsars and mergers, their gravitational-wave emissions may be probed by LIGO-Virgo. Naked inner engines in the latter are of interest to LOFAR surveys, which can be optimized by focusing on the local super-clusters [22], perhaps augmented by planned megaton-neutrino detectors for triggers of supernovae [71] and optical surveys by Pan-STARRs.

Acknowledgements The author gratefully acknowledges stimulating discussions with Alok C. Gupta, Huub Rottgering, Alessandro Spallicci, Robert S. Antonucci, Oliver Jennrich, Gerard 't Hooft and constructive comments from Amir Levinson.

Appendix

For a Kerr black hole in its lowest energy state, the horizon flux of the magnetic field with strength B through a polar cap of half-opening angle θ satisfies

$$\Phi_\theta^e = \pi B \frac{(r_H^2 + a^2)^2}{r_H^2 + a^2 \cos^2 \theta} \sin^2 \theta \quad (33)$$

with $r_H = 2M \cos^2(\lambda/2)$ and $a = M \sin \lambda$. The full horizon flux ($\theta = \pi/2$) $\Phi_H^e = 4\pi B M^2$ is hereby the same for maximal rates and zero-spin. The magnetic flux passing through a polar cap with horizon half-opening angle θ_H satisfies $\Phi_\theta^e \simeq 2\pi B M^2 \theta^2$, about maximal spin (and a factor two larger at zero spin). The Faraday induced potential energy on the flux tube with $A_\phi = B M^2 \theta^2$, is

$$E = e c \partial_t \Phi = e \Omega_H A_\phi \simeq \frac{1}{2} e B M \theta^2 = 2.16 \times 10^{20} B_5 M_9 \theta^2 \text{ eV} \quad (34)$$

in the limit of maximal spin ($\Omega_H \simeq 1/2M$).

To calculate the characteristic lifetime of spin of a supermassive black hole, we estimate the energy dissipation rate $T_H \dot{S}$ in the event horizon permeated with flux during spin-down. Taking the average dissipation rate during the entire process of spin-down to be 1/3-th the maximal dissipation rate, we have

$$D = \frac{c}{3} (\Omega_H A_\phi)^2 = \frac{c}{12} B^2 M^2 = 5.6 \times 10^{47} (B_5 M_9)^2 \text{ erg s}^{-1} \quad (35)$$

The characteristic lifetime of spin for a maximally spinning black hole hereby becomes $T \simeq 29\% \times 2 \times 10^{63} M_9 \text{ erg } D^{-1}$. It defines a correlation $B_5 M_9^{1/2} T_7^{1/2} \simeq 1.04$, or

$$B_5 M_9 = 1.04 \sqrt{\frac{M_9}{T_7}}, \quad (36)$$

whereby (26) results, taking the observed opening angle of 60° in M87 as a fiducial value ($\theta_H = 0.5 \text{ rad}$ [40]).

References

1. Abraham, J., et al., (Pierre Auger Collaboration), 2007, *Science* 318, 938
2. Abraham, J., et al., (Pierre Auger Collaboration), 2008, *Phys. Rev. Lett.*, 101, 061101
3. Aharonian, F., Akhperjanian, A.G., Anton, G., et al. (H.E.S.S. Collaboration), *ApJ Lett.*, to appear, preprint (arXiv:0903.1582)
4. Amati, L., Frontera, F., Tavani, M., et al., 2002, *A&A*, 390, 81A; Nava, L., Ghisellini, G., Ghirlanda, G., et al., 2006, *A&A*, 450, 471; Campana, S., Guidorzi, C., Tagliaferri, G., et al., 2007, *A&A*, 472, 395
5. Antonucci, R., 1993, *ARA&A*, 31, 473

6. <http://brussels2008.aspera-eu.org>
7. Balbus, S.A., & Hawley, J.F., 1991, *ApJ*, 376, 214
8. Baum, S. A., Zirbel, E. L., & O'Dea, C. P. 1995, *ApJ*, 451
9. Bekenstein, J. 1973a, *ApJ*, 183, 657
10. Bekenstein, Jacob D., 1973, *PRD* 7, 2333; Hawking, Stephen W., 1974, *Nature*, 248; A. Strominger, C. Vafa, 1966, *Phys. Lett. B* 379,99
11. Blanchet, L., in these Proceedings
12. Baiotti L., Giacomazzo B., Rezzolla L., 2008, *Phys. Rev. D*, 78, 084033
13. Blandford, R.D., & Znajek, R.L., 1977, *MNRAS*, 179, 433
14. Boldt, E., & Gosh, P., 1999, *MNRAS*, 307, 491
15. Bromberg, O., Levinson, A. & van Putten, M.H.P.M., 2005, *NewA*, 11, 619
16. Chandrasekhar, S., 1983, *The Mathematical Theory of Black holes* (Oxford University Press, Oxford)
17. Carter, B., 1968, *Phys. Rev.*, 174, 1559
18. Chandrasekhar, S., 1960, *Proc. Natl. Acad. Sci.*, 46, 253
19. Della Valle, M., et al., 2006, *Nature*, 444, 1050; Fynbo, J.P.U., et al., 2006, *Nature*, 444, 1047; Gerhels, N., et al., *Nature*, 444, 1044; Gal-Yam, A., et al., 2006, *Nature*, 444, 1053; Amati, L., Della Valle, M., Frontera, F., et al., *A&A*, 2007, 463, 913
20. Dokuchaev, V.I., 1987, *Sov. Phys. JETP*, 65, 1079
21. Eichler, D., & Jontof-Hutter, D., 2005, *ApJ*, 635, 1182
22. Einasto, M., et al., 1994, *MNRAS*, 269, 301
23. Fanaroff, B.L., & Riley, J.M., 1974, *MNRAS*, 167, 31P
24. Farrar, G., & Gruzinov, A., 2008, preprint (arXiv:0802.1074)
25. Ford, L.A., et al., 1995, *ApJ*, 439, 307
26. Frail et al., 2001, *ApJ*, 562, L55
27. Frascchetti, F., 2008, astro-ph/0809.3057
28. Frascchetti, F., & Melia, F., 2008, astro-ph/0809.3686
29. Gehrels, N., et al., 2005, *Nature*, 437, 851
30. Ghirlanda, G., Ghisellini, G., & Lazzati, D., 2004, *ApJ*, 616, 331;
31. Ghisellini, G., Celotti, A., Ghirlanda, G., Firmani, C., & Nava, L., 2007, *MNRAS*, 382, L72
32. Ghisellini, G., et al., 2008, *MNRAS*, 390, L88
33. Goldreich, P., & Julian, W.H., 1969, *ApJ*, 157, 869
34. Gierliński, M., Middleton, M., Ward, M., & Done, C., 2008, *Nature*, 455, 369
35. Greisen, K., 1966, *Phys. Rev. Lett.*, 11, 237
36. Gupta, A.C., Srivastava, A.K., & Wiita, P.J., 2009, *ApJ*, 690, 216
37. Harari, D., 2007, 30th International Cosmic Ray Conference, Merida, Mexico, July 2007; astro-ph/0706.1715
38. Höflich, P.J., Wheeler, J.C., & Wang, L., 1999, *ApJ*, 521, 179
39. Jackson, C., & Wall, J.V., 1999, *MNRAS*, 304, 160
40. Junor, W., Biretta, J.A., Livio, M., 1999, *Nature* 401, 891
41. Kerr, R.P., 1963, *Phys. Rev. Lett.*, 11, 237
42. Komisarov, S., & McKinney, J.C., 2007, *MNRAS*, 377, 49
43. Kumar, P., Narayan, R., Johnson, J.L., 2008, *Science*, 321, 376; *ibid.* 2008, *MNRAS*, 388, 1729
44. Lei, W.H., Wang, D.X., Gong, B.P., & Huang, C.Y., 2007, *A&A*, 468, 563
45. Levinson, A., 2000, *Phys. Rev. Lett.*, 85, 912
46. Levinson, A., in *High Energy Gamma-Ray Astronomy*, 2000, Heidelberg, Germany. AIP Proc., 558. Edited by Felix A. Aharonian and Heinz J. Vlk. (AIP, Melville, New York), p.798
47. Levinson, A., 2006, in *Trends in Black Hole Research*, Edited by Paul V. Kreitler (Nova Science Publishers, Inc., New York, USA), p.119
48. Levinson, A., 2006, *Int.J.Mod.Phys A*, 21
49. Levinson, A., priv. commun.
50. Livio, M., Ogilvie, G. I., & Pringle, J. E. 1999, *ApJ*, 512
51. Lorimer, D.R., et al., 2007, *Science*, 318, 777
52. Lu, F.J., Aschenbach, B., Song, L.M., & Durouchoux, Ph., 2001, *ApSSS*, 276, 141L

53. McKinney, J.C., & Blandford, R.D., 2009, MNRAS, 394, L126
54. Mioduszewski et al., 2004, NRAO/AUI/NSF (<http://www.nrao.edu/pr/2004/ss433/>)
55. Mirabel, I.F., Rodríguez, L.F., 1992, Nature, 358, 215
56. Moskalenko, I.V., et al., 2008, astro-ph/0805.1260
57. Nagar, M., & Matulich, J., 2008, A&A, 488, 879
58. Neronov, A. Yu, Semikoz, D.V., & Tkachev, I.I., 2007, astro-ph/0712.1737
59. O'Dea, C.P., et al., 2008, A&A, to appear
60. Paczyński, B.P., 1991, Acta Astron., 41, 257
61. Page, K.L., et al., 2006, ApJ, 637, L13
62. Pagani, C., et al., 2008, GCN Circ. No. 7426
63. Papapetrou, A., 1951, Proc. Roy. Soc., 209, 248; *ibid.* 259
64. Papaloizou, J.C.P., & Pringle, J.E., 1984, MNRAS, 208, 721
65. Pirani, F.A.E., 1956, Act. Phys. Pol., XV, 389
66. Piran, T., & Sari, R., 1998, in 18th Texas Symp. Relat. Astroph. Cosmology, A.V. Olinto, J.A. Friedman, D.N. Schramm, Eds. (World Scientific, Singapore), pp. 34
67. Reichert, D.E., Lamb, D.Q., & Fenimore, E.E., et al., 2001, ApJ, 552, 57; Reichert, D.E., & Lamb, D.Q., 2001, in Procs. of Gamma-Ray Bursts in the Afterglow Era, ed. E. Costa, F. Frontera, & J. Hjorth (Springer Verlag)
68. Shemi, A., & Piran, T., 1990, ApJ, 365, L55; Rees, M.J., & Mészáros, P., 1992, MNRAS, 258, 41; Rees, M.J., & Mészáros, P., 1993, ApJ, 418, L59; Rees, M.J., & Mészáros, P., 1994, ApJ, 430, L93; Mészáros, P., & Rees, M.J., 1997, MNRAS, ApJ, 476, 232; Wijers, R.A.M.J., Rees, M.J., & Mészáros, P., 1997, MNRAS, 288, L51; Reichart, D.E., 1997, ApJ, 485, L57; Piran, T., 1998, Phys. Rep., 314, 575; Piran, T., 1999, Phys. Rep., 314, 575; Piran, T., 2000, Phys. Rep., 333, 529; Garcia, M.R., Callanan, P.J., & Moraru, D., et al., 1998, ApJ, 500, L105; Mészáros, P., 2002, ARA & A, 40, 137
69. Ruffini, R., & Wilson, J.R., 1975, Phys. Rev., 12, 2959
70. Semenov, V., Dyadechkin, S., & Punsly, B., 2005, Science, 305, 978
71. Shin'ichiro, A., Beacom, J.F., & Hasan, Y., 2005, Phys. Rev. Lett., 95, 171101
72. Stephani, H., 1990, General Relativity, 2nd Ed. (Cambridge: Cambridge University Press)
73. Stefani, F., Gerbeth, G., Gundrum, T., et al., 2009, preprint (ArXiv: 0904.1027v1)
74. Tanaka, Y., Nandra, K., Fabian, A.C., et al., 1995, Nature, 375, 659; Iwasawa, K., Fabian, A.C., Reynolds, C.S., et al., 1996, MNRAS, 282, 1038; Narayan, R., McClintock, J., & Shafee, R., 2007, in Astrophysics of Compact Objects, eds. Y. F. Yuan, X. D. Li, D. Lai, AIP Conf. Proceedings
75. Thorne, K.S., Price, R.H., & McDonald, D.H., 1986, *Black Holes: The Membrane Paradigm* (Yale University Press, New Haven, CT)
76. Troja, E., et al. 2007, ApJ, 2007, ApJ, 665, 599
77. Urry, C.M., & Padovani, P., PASP, 107, 803
78. van Putten, M.H.P.M., & Wilson, in Proc. Astrophysical black holes: Theory confronts Observations, <http://www.kitponline.com/>
79. van Putten, 1999, Science, 284, 115
80. van Putten, M.H.P.M., 2000, Phys. Rev. Lett., 84, 3752
81. van Putten, M.H.P.M., & Ostriker, E.C., 2001, ApJ 552 L31
82. van Putten, M.H.P.M., 2001, Phys. Rev. Lett. 87, 091101
83. van Putten & Levinson, A., ApJ, 584, 937; van Putten, M.H.P.M., 2003, 583, 374 *ibid.* 2004, ApJ, 611, L81; *ibid.* 2008, ApJ, 685, L63;
84. van Putten, M.H.P.M., 2002, ApJ, 575, L71
85. van Putten, M.H.P.M., 2004, ApJ, 611, L81
86. van Putten, M.H.P.M., 2005, Nuov. Cim. C, 28, 597; *ibid.* 2008, ApJ, 685, L63
87. van Putten, M.H.P.M., 2005, *Gravitational Radiation, Luminous Black Holes and Gamma-Ray Burst Supernovae* (Cambridge: Cambridge University Press)
88. van Putten, M.H.P.M., Gupta, A.C., 2009, MNRAS, 394, 2238
89. van Putten, M.H.P.M., 2009, MNRAS Lett., doi:10.1111/j.1745.3933.2009.00666.x
90. Velikhov, E.P., 1959, Sov. Phys. JETP, 36, 995

91. Véron-Cetty, M.-P., & Véron, P., 2006, *A&A*, 455, 733
92. Villaseñor, J.S., et al., 2005, *Nature*, 437, 855; Fox, D.B., et al., 2005, *Nature*, 437, 845; Hjörth, J., et al., 2005, *Nature*, 437, 859
93. Workman, J., & Armitage, P., 2008, *ApJ*, 685, 406
94. Wald, R.M., 1974, *Phys. Rev. D*, 10, 1680
95. Waxman, E., 2004, *Pramana* 62, 483 (Proc. PASCOS 2003, Mumbai, India), preprint (arXiv:astro-ph/0310079)
96. Woosley, S.L., 1993, *ApJ*, 405, 273; Paczyński, B.P., 1998, *ApJ*, 494, L45
97. Zatspein, G.T., & Kuzmin, V.A., 1966, *Soviet Phys.-JETP Lett.*, 4, 78
98. Zaw, I., Farrar, G.R., & Greene, J.E., 2008, preprint (arXiv:0806.3470)